Experimental and Numerical Analysis of Unsaturated Soil Slope Stability with Rainfall and Jute Fibre Reinforcement Condition

Saurabh Kumar[1] and Lal Bahadur Roy[2]
[1]*Research Scholar,* [2]*Professor, National Institute of Technology, Ashok Rajpath, Patna 800005, India*
Email: saurabhk.phd19.ce@nitp.ac.in

ABSTRACT: Rainfall has become a main trigger of slope failure for embankments in most coastal areas. The common slope stability analysis is incapable of accurately forecasting slides where suction pressures play a critical role. This realization is used for elaborate stability analyses, which include mesh and suction to better predict rainfall-induced slides at effective slopes. Jute fibre is one of the reinforced materials which is utilized to improve soil strength. Accordingly, the present study explores to study the effects of slope inclination on soil stability and the collected soil samples using jute fibre in artificial rainfalls. Therefore, this article presented various assessments for soil sample testing. Different tests like sieve analysis, permeability test, direct shear test (DST), liquid limit, plasticity limit, and numerical modelling were conducted in the laboratory. Geo-studio 2021 is the software utilized for numerical and experimental modelling. The findings of the research revealed that the failure is caused by a soil suction loss when the inclination of the slope is higher than the soil friction angle. Subsequently, when the inclination of the slope is lower than the soil's friction angle, the collapse is caused at the slope's toe due to the improvement of the positive water pressure. Furthermore, when the slope angle increases, slopes are becoming increasingly vulnerable to rapid collapse under rainfall. Consequently, the article studies the jute fibre which is combined with soil to improve its soil performance while using two rows, three rows, and four rows of jute. This estimation results that the jute fibre performs better than the without using jute fibre under different rainfall conditions. According to the findings, the random distribution of jute fibres had a favourable influence on both strength measurements and safety aspects. Utilizing the factor of safety and matric suction, the performance of jute fibre is superior to those without using jute fibres. Consequently, the proposed work improves the stabilization of soil, and factor of safety with jute fibre in rainfall conditions.

Keywords: Soil samples, Slope stability, Reinforced material, Jute fibre, Sieve analysis, Factor of safety, Matric suction, Deformation.

1. INTRODUCTION

Every year, thousands of landslides occur around the world, instigating massive financial losses and even fatalities in extreme circumstances. Landslides on slopes have always been an important topic. Due to these landslides, the stability of the slope is a very important process for slope embankment. The embankments are usually built in several phases; during these constructions, the stability of the ground soil is ensured. To effectively quantify the gain of shear strength in the field of geotechnical engineering practice, the undrained shear strength of foundation soil is normally rising with consolidation [1]. During rainstorms, the top layer of the soil in an embankment slope is more sensitive to erosion. It provides minimal erosion resistance and rapidly reduces the strength of the soil [2]. Therefore, reinforced embankments increase the bearing capacity of the soil and reduce the displacements in the vertical and lateral planes [3]. Soil stabilization is a technique of enhancing the physical, chemical, or biological qualities of natural soil to relate to engineering requirements. A direct shear test is utilized to determine the shear strength qualities, cohesiveness, and friction angle, which is performed in a laboratory [4]. The finite difference approach was utilized to perform the numerical modelling, and the model scale is used to replicate the centrifuge tests in the numerical modelling [5].

Due to the high expense of creating and transporting free-draining coarse-grained materials, the slope failure along highways is frequently repaired or restored using locally available soils that significant amounts of fines (clay and silt) are presented in [6]. A geocell-reinforced slope acts as a beam in the soil because of the three-dimensional nature of the reinforcement, which includes height. Furthermore, the moment of inertia is taken into consideration due to its bending features, resulting in enhanced bending strength, the reinforcement lowers slope displacement and increases the factor of safety (F.S) of slope [7]. Jute fibres are compared to the usual strength qualities of soil. Jute fibres of predefined length and content are mixed extensively with expansive soil until a fairly uniform distribution of jute fibres in the soil is achieved for fibre-reinforced soil specimens that are randomly distributed [8]. The utilization of fibre is termed the physical form of soil stability. The fibre-reinforced soil is the discrete elements, and randomly distributed components, such as fibres are incorporated by the soil mass. Fibres improve the mechanical properties of soil composites [9].

The reinforcing effect location on the failure and deformation behaviour of soil slope and superstructure is explored by evaluating various geogrid layers [10]. Jute fibre is excellent for enhancing soil qualities because it is inexpensive, readily available, biodegradable, and environmentally friendly [11]. When it is a low-cost, locally available material, this can be hypothesized that supporting the soil using jute-geotextile [12]. Utilize a moisture barrier and recycled plastic pins that have been altered to stabilize the pavement distresses and the rainfall-induced slope failure [13]. The chance of failure or F.S. of slopes is displayed due to providing the output file in ASCII format [14]. Then the matric suction losses caused by rainfall infiltration had only a minor impact on the global and local F.S. of the reinforced sand slopes. The tensile reinforcement strengths are necessary to sustain F.S. on reinforced clay and silt slopes [15]. Than Nguyen et al. [16] presented a probabilistic analysis to assess the stability of unsaturated soil slope under rainfall. Assumptions of reducing soil shear strength and increasing the unit weight of the soil were made in the analysis. Later in [17], Nguyen presents a probabilistic framework for slope stability analysis considering the spatial variability of root reinforcement. Kumar et al. [18] provide a brief explanation of geotextiles with their uses in construction, toxicity, performance, and their types. From a geotechnical standpoint, problematic soils are those that can disperse, collapse, have an excessive settlement, expand, or even fail under relatively modest stress conditions. Soil erosion or cracking is occurring in the soil due to these issues; the soils are not stable for the embankment. Due to these problems, this paper presents various testing methods for analysing the stability of slope soil. Here, rainfall intensity is set up to test the soil stability, because of this, some cracks and slope failure will occur. Based on this, reinforced material like jute fibre is added to strengthen the soil and increase slope stability.

A recent study about soil stability based on reinforced soil is reviewed in this section. Mamat et al. [19] provided the road's embankment slope stability constructed on soft ground with prefabricated vertical drains (P.V.D.s). The slope stability was evaluated based on the factor of safety (F.O.S.) through numerical analysis and modelled with an artificial neural network (ANN). For ANN model training, a dataset is developed using a comparative analysis between numerical simulation and field data was employed to verify the smear effect's permeability ratio.

A novel approach is proposed by Li, Y. X, et al. [20] to determine the F.S. of soil slopes when the soil strength follows the nonlinear yield criterion. First, the magnitude and coordinate of minor primary stress are determined using numerical simulation. A combination with the nonlinear failure criterion was utilized to determine the equivalent strength parameters. Finally, the upper bound theorem was utilized to calculate the F.S. and the discretization technique was used to create the slip surface. The effect of polypropylene fibres on the stability of embankment slopes subjected to freeze-thaw cycles was investigated by the numerical analysis method by Gong et al. [21]. The orthogonal experiments of three levels and the three factors (freeze-thaw cycle, fibre content, and fibre length) were carried out, and DST was used to measure the nine sets of specimens and shear strength metrics such as bond force and internal friction angle.

Luo et al. [22] investigated the failure and deformation behaviours of reinforced slopes with various geotextile layouts utilizing a set of drawdown centrifuge model experiments. Under drawdown conditions, the slope failure feature is changed, displacement is minimized, and to considerably raise the ductility and safety limit using the geotextile reinforcement, as also examines the failure and deformation of reinforced and unreinforced slopes. The injection approach was used to produce one untreated embankment, and three small-scale bio-treated sand embankments are investigated by Wang et al. [23]. To investigate the slope of the failure embankment, rainfall scouring experiments were then conducted. The biotreated sand embankment's scouring/erosion resistance was much better than the untreated sand embankments revealed in the experimental results. While increasing the treatment cycles, the failure time of the embankment is also increased.

The utilization of jute fibre treated with sand is used to improve the engineering properties of soil focused on by Sharma et al. [24]. In this instance of earthen slopes and pavement, the jute fibre is treated with sand to improve engineering properties. The jute geotextile can be used as soil reinforcement or stabilizer, as determined by this study. Based on five synthetic rainfall patterns derived from actual heavy rainfall events, the slope stability of an agricultural embankment was evaluated by Park, et al. [25]. In practice and hydrological design, common patterns of rainfall hyetographs were used to create rainfall patterns. The limit equilibrium process was utilized to compute the embankment's stability. Under rainfall patterns, the time-series slope instability is revealed by the results of the stability analyses, and particularly the rainfall pattern that caused the most instability to the embankment was identified.

Adimilli et al. [26] determined the likelihood of soil slope failure when slopes of various angles were subjected to heavy rainfall. In a model test tank, slopes of 30, 45, and 60° were created. In the event of heavy rainfall, the 60° slope was discovered to be extremely vulnerable to failure. In addition, to improve the 60° slope by strengthening it with a low-cost natural geocell (bamboo geocell), the current study attempt. On the surface of the 60° slope, a bamboo geocell with a thickness of 50 mm was installed. After being exposed to a sustained period of around 13 hours of heavy rainfall, it was clear that the 60° slope was protected with bamboo geocell. A digital image-based triaxial shear test system was used to evaluate the dry–wet action on mechanical behaviour and failure mode of basalt fibre–reinforced loess by Wu. Z. et al. [27]. The shear strength of fibre-reinforced loess falls following dry-wet cycles, although it shows inverted U-shaped variations with fibre content, with 0.6% fibre content providing the best resistance to dry-wet action. The fibre-reinforced loess samples have fewer fractures than the unreinforced loess samples, showing that fibres are effective at limiting the initiation and spread of apparent cracks. After fibre addition, the failure mechanism shifts from brittle shear failure to overall bulging.

Zhang et al. [28] proposed a method for analysing the probabilistic stability of embankment slopes under transient seepage that took into account both the spatial variability of soil characteristics and seismic unpredictability. The random field theory describes the spatially variable soil characteristics in the sense that a large number of random field samples of the soil parameters can be easily created. The pseudo-static method of seismic stability analysis is used to determine the factor of safety (F.S.) of the embankment slope under seismic conditions corresponding to each random field sample. The horizontal scale of fluctuation, as well as the coefficient of variation of the friction angle, has a more substantial influence on the chance of embankment slope failure and is evaluated based on the results.

Jirawattanasomkul et al. [29] establish an in-depth understanding of the compressive behaviour of concrete confined with low-cost natural fibre-reinforced polymer (N.F.R.P.). The results prove that N.F.R.P. is effective and suitable to enhance the confinement effect of concrete, especially Jute-NFRP. Later, Jirawattanasomkul et al. [30] presented an improvement of jute fibre–reinforced polymer (J.F.R.P.) composites by heat treatment. The heat treatment conditions (i.e., temperature and duration) were considered. The experimental results indicated that a suitable heat treatment condition of 80°C for 24 h can significantly increase the tensile strength of J.F.R.P. coupons and the compressive strength of JFRP-confined concrete. Subsequently, Jirawattanasomkul et al. [31] examined the use of natural jute fabric reinforced polymer (J.F.R.P.) composite sheets as external strengthening material of reinforced concrete (R.C.) beams. The test results revealed that J.F.R.P. can significantly improve the shear strength capacity of beams. The use of eco-friendly building materials and/or recycling technologies becomes a trend in the construction industry. Accordingly, [32] explores the development and use of water hyacinth wastes for producing fibre-reinforced polymer composite as a strengthening material to confine concrete. It is concluded that the mechanical properties of water hyacinth fibre-reinforced polymer composite are acceptable for concrete strengthening purposes.

Nguyen et al. [33] suggested the effect of root reinforcement on the stability of vegetated slopes under rainfall conditions. The results show that the contribution of root cohesion to slope stability was more significant for the non-compacted soil condition than for the well-compacted one. Both modelled and monitored pore-water pressure reached the highest values about 1 d after the daily rainfall had reached its peak. Komolvilas et al. [34] presented a comprehensive failure analysis of local rainfall-induced landslides based on topographical and geological information. Rainfall measurement data were gathered from two rainfall stations close to the study area. The slope stability analysis and rainfall records revealed that the Huay Khab landslide was mainly caused by an increase in the water content of residual soils due to the prolonged rainfall, which led to a sharp decrease in the shear strength.

Ongpaporn et al. [35] investigated the performance of the bioengineering techniques employed at Ban Na Tum utilizing 3D stability-seepage modelling. The analysis results revealed that the critical locations on slopes (i.e., the lowest factor of safety) were not necessarily stationary but could change with ongoing water infiltration and seepage. Maryanto et al. [36] presented an effort to overcome the urban heat island phenomenon (UHI) in buildings. Sago midrib fibre is a natural composite material used as a reinforcing material for natural composite materials due to its thermal and mechanical properties. The results showed an increase in the impact value of natural composite materials reinforced with sago midrib fibre with variations in NaOH levels and the resin–catalyst matrix.

Kumar et al. [37] studied the influence of jute fibre reinforcement with the help of three case studies. The first case study described laboratory model testing and numerical analysis performed on a modelled slope that simulated an existing embankment that failed on many occasions following overnight heavy rainfall. The second case

study discussed how vegetation may minimise the likelihood of soil separation and the velocity of surface run-off by decreasing surficial soil erosion. Jute geotextiles have excellent hydrophilic characteristics that aid plant development; for this reason, they were used in the case study. The third case study developed a multi-fibre approach to traditional geotextiles to create an eco-sustainable product(s) with superior geotechnical qualities for improving the efficiency of earthen structures using soft revetments. The presence of jute fibre geotextiles results in better performance in the stabilisation of soil and the minimum value of deformation and maximum value of the factor of safety. This evidence revealed that the N.F.R.P., especially J.F.R.P., has been well accepted as a strengthening material for R.C. structures. However, the application of J.F.R.P. composites in slope inclination on soil stability and the collected soil sample's damaged shear during seismic events has not yet been evaluated to ensure their effectiveness and structural performance. Consequently, the article study analyses the jute-reinforced slope with various tests for the soil samples. The remaining part of the article is well-structured as follows; section 2 elucidates the proposed methodology of the study. Section 3 displays the experimentation and results in the discussion part, and section 4 reveals the conclusion of the study, respectively.

2. PROPOSED METHODOLOGY

In this study, experimental laboratory-scale microcosms are developed to investigate the slope failure of untreated and bio-treated sand embankments under rainfall conditions. The test sand was taken from a construction site and sieved in a laboratory to remove any unexpected large grains. The water content and dry density of the soil, height, and gradient of the slope were kept constant throughout the model tests. The behaviour influence of reinforced slopes is observed utilizing different geotextile layouts. Jute fibre has emerged as a strong alternative to synthetic geotextiles for many civil engineering applications. Due to their short life span, jute fibres are used as a separator, vegetation growing mesh on slopes or vertical drains. Consequently, the study utilized jute fibre with and without experiment in the effective slopes. In this experiment, disturbed and undisturbed samples are utilized for the study. During the sampling process, the soil's natural structure has been altered or destroyed, the natural structure is referred to as disturbed samples which are referred to as representative samples. Soils from different strata mixed are the non-representative samples. In addition, the dead weight of the soil slope is applied to the entire slope, and the evenly distributed loading is applied to replicate the vehicle load are the two types of loadings that were used in the finite element model in the slope stability analysis. The flow diagram of the proposed research is depicted in the subsequent figure 1.

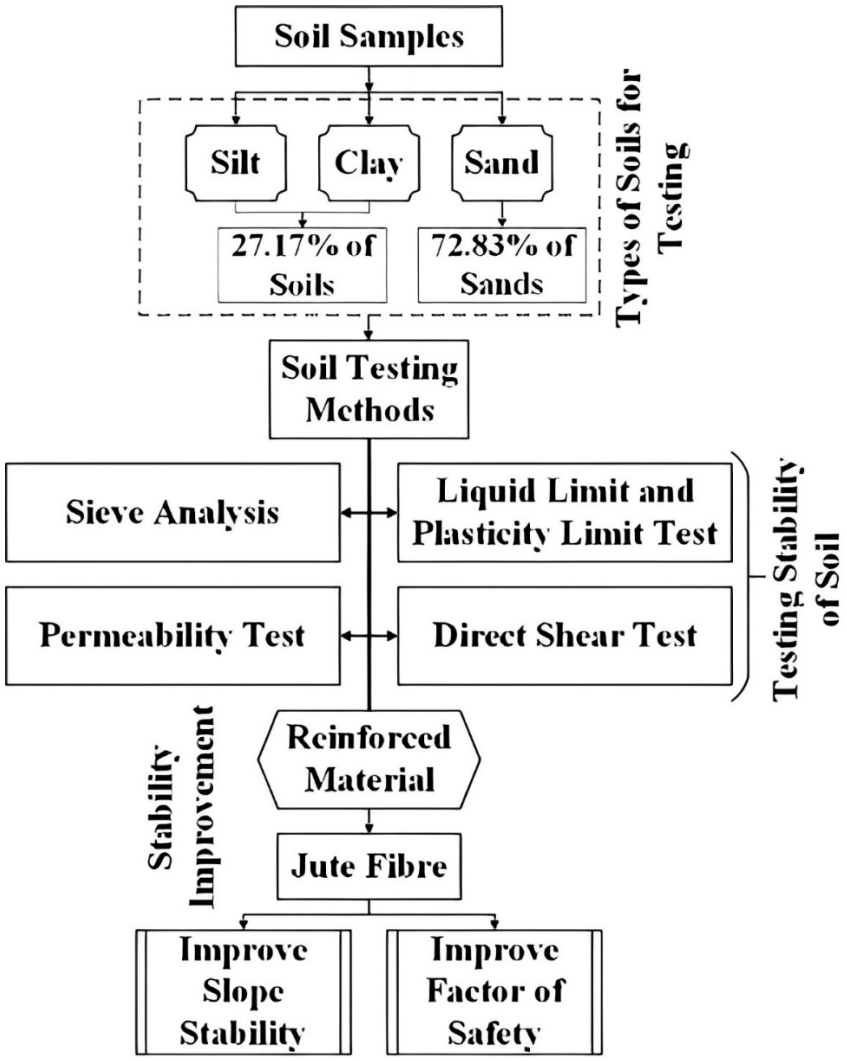

Figure 1 Flow diagram of research methodology

2.1 Material Collection

Soil sampling is represented as the procedure of obtaining tiny soil samples, which are used to determine the soil embankment stability. There are 27.17% of silt and clay soil samples and 72.83% of sand materials taken for this study. Multiple smaller samples composed an accurate soil sample known as cores. The majority of their nutrients are derived from plants or grasses, that individual cores contain soil from the surface. In a variety of locations throughout the area, a minimum of ten soil cores were taken and included in the final samples of each area. Where several tests are conducted to measure the stability of soil slope. Soil samples are powdered, sieved, and dried before being analyzed. During this analysis, a homogenous mixture was ensured by grinding and sifting steps. Soil samples are dried at 50°C in cardboard boxes. In a pestle and a mechanical mortar, the dried soil is ground and passed through the 12-mesh (approximately 2 mm.) screen. The testes are then discovered in this study.

Mineral particles, water, air, and organic matter are all present in these soils. Based on these combinations, the soil properties are determined by the chemistry, colour, structure, porosity, and texture of the soil. Table 1 illustrates soil sample properties like the plastic limit, liquid limit, plasticity index, coefficient of permeability, dry unit weight, saturated unit weight, cohesion, angle of internal friction, Poisson's ratio, and young's modulus of elasticity. These are the soil properties utilized in the experiment, and there are various soil testing methods are utilized to test the soil stability. Specified analytical equipment is utilized for the analysis, and the samples are prepared into a form ready to complete the treatment. Sample preparation could include Sample clean-up, sample pre-concentration, alkali or acid-based chemical digestion, sample extraction, crushing, and dissolution, respectively.

Table 1 Soil samples properties

Soil Properties	Values
Plastic Limit, W_p	15 %
Liquid Limit, W_L	21 %
Plasticity index, $P.I$	6 %
Soil classification	SM-SC
Coeff. of Permeability, K_{sat}	3.27 x 10^{-4} cm/sec
Dry unit weight, γ_{dry}	14.8 kN/m^3
Saturated unit weight, γ_{sat}	17.5 kN/m^3
Cohesion, C	0.4 kPa
The angle of internal friction, ϕ	25.45°
Young's modulus of Elasticity, E	5110 kPa
Poisson's ratio, ϑ	0.25

The soil properties and their values are explained in table 1 and are depicted as follows. Due to the moisture weight, the alteration between the dry and wet weights is recorded.

2.1.1 Procedures for Sample Preparation

Approximately 115 grams of the material transient to the No. 400 mm screen is obtained from an illustrative air-dried sample soil. The soil is separated into two portions; several 400 mm sieves were used. A pestle and mortar are utilized to retain fractions without re-sieve and

fracturing individual grains and to break apart soil aggregations. Until just a little amount of material passes through the sieve, regrind the remaining material. Remove the stuff that has remained on the sieve and discard it. Before determining the L.L. and P.L., recombine the sections that passed through the No. 400 mm sieve and thoroughly mix them.

2.2 Reinforced Material for Slope Stability

Slopes can be stabilized by adding a surface cover, excavating, and modifying (or regrading) the slope geometry, and reinforcing the slope with support structures. Continuous fibres are woven, stitched, braided, or knitted into the fabric from twisted and plied yarn to create multidirectional reinforcements. Almost any reinforcing fibre can be utilized to create fabrics. The fabrics are created with the utmost standard materials like carbon, aramid, and fibreglass. Enhancing its resiliency and strength by including reinforced material in the soil is involved in the method of soil stabilization. The vetiver plant is a very simple, practical, Phyto-remediation, low-cost, low-maintenance, and very successful method of water and soil conservation and land stabilizations and rehabilitation. When planted in single rows, vetiver plants will form a hedge which is very effective in slowing and spreading run-off water, reducing soil erosion, conserving soil moisture, and trapping sediment and farm chemicals on site. The extremely deep and massively thick root structure of the vetiver binds the soil and makes it impossible for it to be removed under high-velocity water flows. Vetiver is drought resistant and ideal for the stabilization of steep slopes because of its deep and fast-growing root structure. On a small scale, directly using this Vetiver plant in a laboratory experimental setup is extremely challenging. Scale modelling should be used with jute fibre, instead of using Vetiver roots. The mechanical qualities of the vetiver plant are scaled according to the strength and other features of the jute.

2.2.1 Jute Fibre for Slope Stability

Jute fibre is widely known for its ability to be turned into coarse and strong threads, and it is a type of plant fibre. Individual jute fibres are noted for their glossy, long, and soft nature. Plants of the genus Corchorus are thought to be involved in the production of this fibre. Jute fibre can be utilized to strengthen the soil and improve engineering qualities. To endure rot and heat, jute fibre is utilized because of its ability, high tensile strength, and superior durability as well as excellent drainage and filtration provided by porous texture. Jute is also inexpensive, readily available, biodegradable, and environmentally beneficial. Preventing lateral deformation, and reducing settlement, ductility, bearing capacity, and strength are improved by the soil mass reinforcement. Stabilized soils have strong compressive strength, less post-peak strength loss, higher extensibility, no weak planes, and isotropy in strength. Jute is biodegradable and poses no threat to the environment.

Jute has the highest tensile strength of natural fibres and can withstand rolling and heat. Fibre provides a high level of fineness and flexibility because good pliancy is possessed by fibres and render. Jute is a suitable fibre for geosynthetics because of its strong torsional rigidity, consistent tenacity, high initial modulus, and low percentage of elongation-at-break. Due to the greater cellulose content, jute can absorb water, which is another notable feature. Their dry weight of water is up to 500%, it is absorbed by the jute fibres/yarns. Jute has the highest hygroscopic quality of natural and man-made fibres. To meet specific requirements for tensile strength, porosimetry, transmissivity (water flow through the fabric), and permittivity (water flow across the fabric) are all customized by Jute Geotextiles, which are similar to man-made geotextiles. Jute Geotextiles have a similar break and burst strength which is close to man-made geosynthetics. It also provides a particular environmental advantage. Jute fibres were obtained at the city of Jodhpur's market. The fibres are cut into 20 mm long pieces and combined by dry soil weight in percentages of 0.5%, 1%, 1.5%, and 2%.

Figure 2 Jute fibre in slope stability

The usage of jute fibre for soil reinforcement is crucial to increasing slope stability. Figure 2 represented the jute fibre utilized for slope stability. The mechanical qualities of the vetiver plant are scaled according to the strength, and other features of jute, and the feature of these jute fibres are expressed as follows.

2.2.2 Jute Fibre Characteristics

- ❖ It is environmentally friendly due to this 100% recyclable and biodegradable.
- ❖ Golden Fibre is another name for jute fibre due to its silky shine and golden natural fibre.
- ❖ It is derived from the skin or plant's stem bast because of its cheapest vegetable fibre.
- ❖ Cotton is the first important fibre subsequently, jute is also a significant vegetable fibre, it is global consumption, usage, availability, and production.
- ❖ It allows fabrics to have breathability, low extensibility, and high tensile strength. As a result, jute is ideal for bulk packaging of agricultural commodities.
- ❖ Antistatic qualities, high insulation, moderate moisture desorption rate, and thermal conductivity are low are the advantages of jute.

2.2.3 Jute Fibre's Mechanical Properties

In terms of fatigue and mechanical properties, balanced the woven jute hybrids like environmentally friendly materials, which are cost-effective, and light-weighted. Consequently, many applications, particularly those with modest cycle stress loads, are advised to reduce their reliance on synthetic fibres. "Experimental and CLT approaches are used for evaluating the elastic properties of jute fibre."

Table 2 Jute fibre's mechanical properties

Characteristics	Values
Density, ρ	1.35 gm/cc
Young's Modulus, E	5110 kPa
Poisson's Ratio, ϑ	0.25
Shear Modulus, G	7.24 GPa
Tensile Strength, T	393 MPa

Table 2 depicts the mechanical properties of jute fibre; it is very essential to determine the deformation and F.S. of the slope. The mechanical properties values for jute fibre are density is 1.35 gm/cc, Young's Modulus is 5110 kPa, Poisson's ratio is 0.25, Shear Modulus is 7.24 GPa, and Tensile Strength is 393 MPa, respectively.

3. EXPERIMENTATION AND RESULT DISCUSSION

The experimentation setting of the research work shows that all slope models were created in a specially designed chamber. The slope failure of untreated and biotreated sand embankments under rainfall conditions is investigated in this work using experimental laboratory-scale microcosms. The initial ratio of the slope is 2:1, and it contains a rainfall nozzle, frame, inlet pipe, outlet pipe, rain gauge, and Digital Tensiometer are presented. Initially, the soil samples are set up in slope format. Here, the rainfall intensity is fixed in the experiment to test the slope soil stability. There are rainfall nozzles, inlet pipes, and outlet pipes utilized for rainfall intensity. After the rainfall intensity, there are cracks are appearing on the soil, and slope failure has occurred. A rain gauge is utilized to measure the rainfall, and the digital tensiometer is used for measuring the matric suction of soil the testing program was established, and fibre inclusion uniformity has a direct impact on the reinforcing effect of fibre-reinforced soil. The effect of treatment on the rainfall infiltration process in the embankments is further studied using numerical simulation utilizing the finite element method (F.E.M.). The fundamental process for improving scouring/erosion resistance in biotreated sand embankments, as well as the slope failure characteristics of treated sand embankments, are discussed.

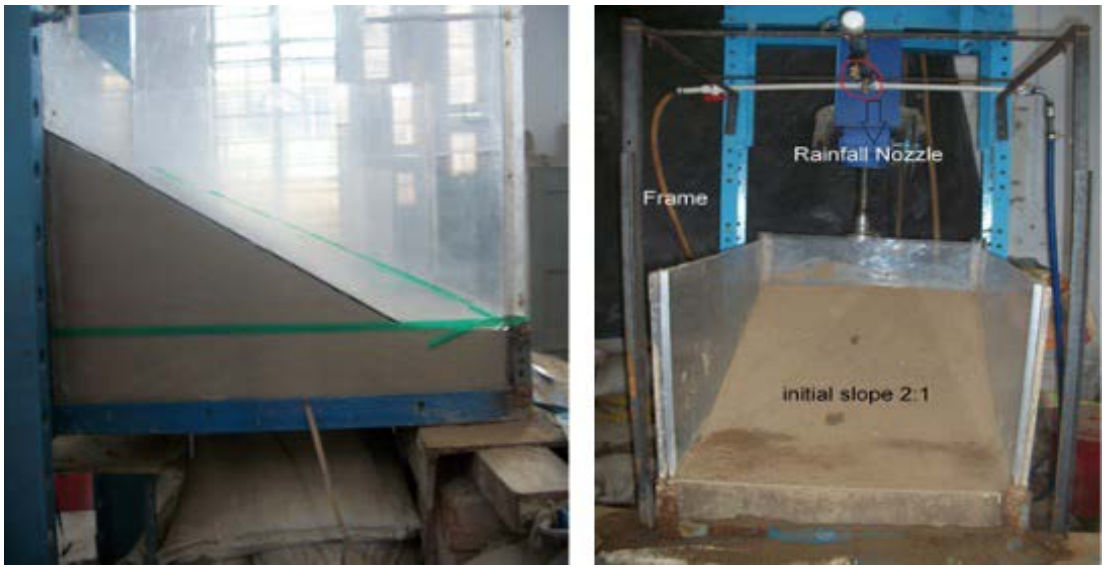

Figure 3 Experimental setup of the research

Figure 3 displays the experimental setup of the proposed work; this is utilized to test the slope soil stability. A brief explanation of this experimental setup is described above. Subsurface investigations, instrumentation and monitoring, report documentation, laboratory testing and analysis, site visits, and engineering studies and design may all be part of slope stability evaluations. Due to the rainfall intensity, there are cracks on slope soils appear, and the failure is caused. Measuring matric suction and rainfall are given as follows.

The standard instrument rain gauge is 203 mm, and an 8-inch is utilized for rainfall measurement. This is a fundamentally 203 mm diameter circular funnel that collects rain into a calibrated and graduated cylinder. Precipitation up to 25mm can be recorded by the measuring cylinder. The free energy shifts in a unit volume of water, known as matric suction, which occurs when isothermally transitioning from the soil water condition to the free water state (unit: kilopascal), is described as the fundamental volume of soil, water, and air.

3.1 Rainfall and Matric Suction

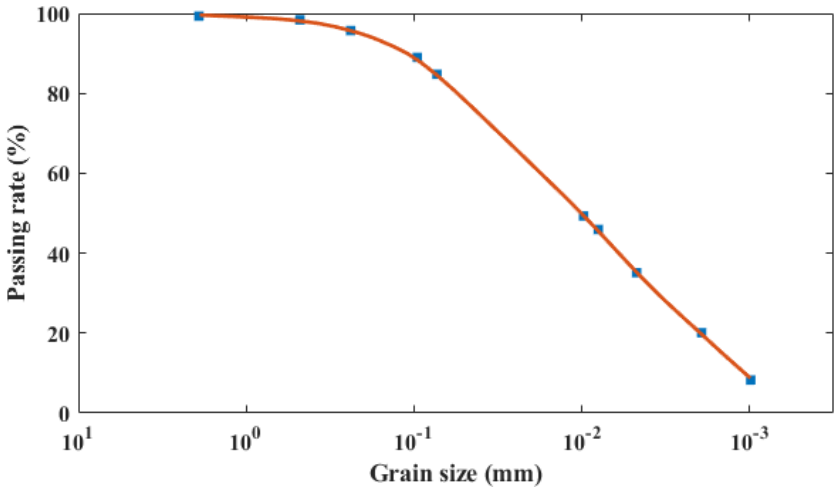

Figure 4 Grading curve of expansive soil

Figure 4 reveals the grading curve of expansive soil. The testing program included fine-grained silty clay soil and various sand components. Based on the value range of the free swell index, the chemical contents, and the grain size distribution curve of the soil analysed acquired through a series of indoor soil mechanics tests and different analyses, it could be determined that the soil utilized in this study was typical weak expansive soil.

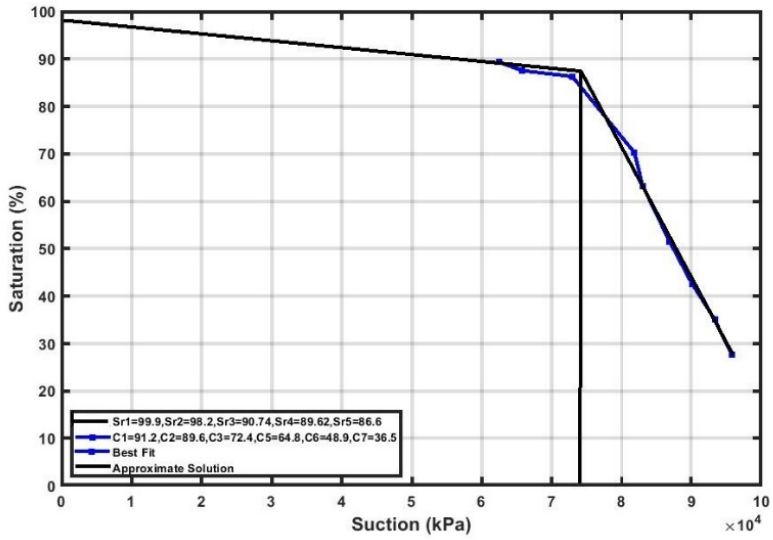

Figure 5 Soil water characteristics curve from clay

Figure 5 depicted the soil water characteristics curve from clay, which is developed based on the experimental data using moisture content and soil suction. The procedure is used to evaluate these soils, which have around 800 kPa. This is greater than the maximum suction values considered in this study (from the limit equilibrium analyses presented later), so only the saturated portion of the strength envelope is needed in the current study.

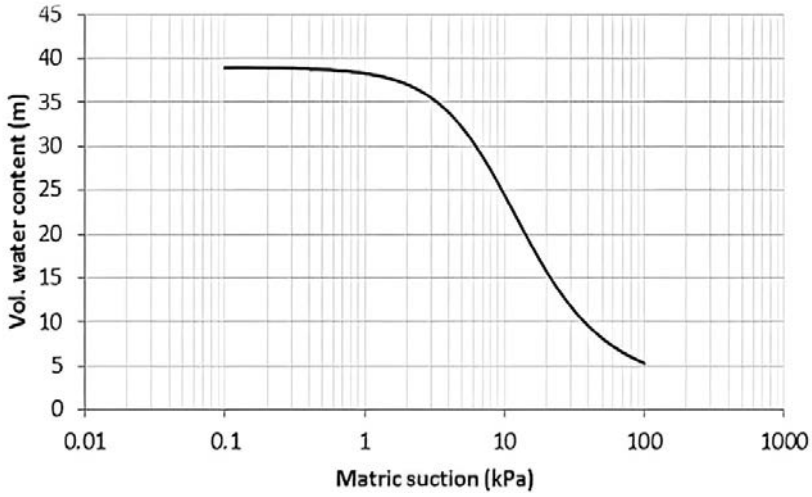

Figure 6 Matric suction for volume of water content

Figure 6 demonstrates the matric suction graph for the volume of water content. However, these modellings consider the influence of changes in water content or matric suction.

Subsequently, the specimens were unaffected by changes in water content if compacted at the optimum or wet of optimum soil moisture content; the results showed that regardless of the level of matric suction. The matric suction is increased by decreasing the volume of water content.

3.2 Laboratory Testing

A soil test is important for several reasons in this study soil testing is important for testing the embankment soil stability. The various laboratory testing methods for soil samples like sieve analysis, permeability test, direct shear test, and lime limit and plastic limit test. A detailed explanation of these testing is given as follows.

3.2.1 Sieve Analysis for Soil Sample Test

In chemical and civil engineering, a sieve analysis or gradation test is a procedure or practice used for particle size distribution determination, also known as the gradation of granular material using a sequence of sieves with increasingly lower mesh sizes, and each sieve blocked the quantity of material is expressed as a total mass percentage. For all aggregate technicians, sieve analysis is a basic test that is often recognized as the gradation test.

The test is performed by stacking a series of sieves with decreasing mesh sizes on top of each other and passing the soil sample via the sieve "tower. Consequently, the different sieves retaining the soil particles are distributed. In this study, the soil sample weight is 500 gm. Arrange the sieving in descending order like 4.75 mm, 2.36 mm, 1.18 mm, 600 μm, 425 μm, 300 μm, 150 μm, and 75 μm.

The weight of the sample after washing it through a 75 μm sieve is 364.15gm.

$$75\mu m = \frac{500-364.15}{500}\% = 27.17\% \quad (1)$$

Through the 75 µm, the soil is passing it is 27.17 % of soil samples are silt and clay soils.

Table 3 Results of sieve analysis

Sieve Size	Empty Wt. of Sieve (gm.)	Sieve + Sample Wt. (gm.)	Sample Retained (gm.)	% Retained	Cumulative % Retained	% Finer than
4.75 mm	482	482.45	0.45	0.09	0.09	99.92
2.36 mm	421.3	426	4.8	0.96	1.05	98.95
1.18 mm	406.8	430.9	24.2	4.84	5.88	94.15
600 µm	396.7	465.1	68.5	13.7	19.59	80.41
425 µm	348.2	401.7	53.6	10.72	30.31	69.69
300 µm	387.9	460	72.2	14.44	44.75	55.25
150 µm	342.2	466.3	124.2	24.84	69.59	30.41
75 µm	321.3	337.4	16.2	3.24	72.83	27.17
Pan	397.6	398.7	1.3	27.17	100	0

Table 3 described the sieve analysis for the soil sample. Initially, the sieve size is 4.75 mm to 75 μm. It also describes the sieve's empty weight, sieve, and sample weight, sample retained, percentage of retained, cumulative retained, and finer than values are detailly described in the table. Based on these results, classifications of soil samples were represented as follows.

The sieve analysis result shows that D_{60} is 0.38 mm, D_{30} is 0.19 mm, and D_{10} is 0.037 mm. The soil sample is evaluated as well-graded according to the I.S.: 1498-1970 code. Most of the water passes through 4.75 mm, thus, it is sand, and more than 12% passes through 75 μm. Therefore, the Coefficient of curvature and Coefficient of uniformity is depicted as follows,

$$C_c = \frac{D_{30}^2}{D_{60} \times D_{10}} = 2.57 \quad (2)$$

$$C_u = \frac{D_{60}}{D_{10}} = 10.27 > 6 \quad (3)$$

Therefore, C_c lies between 1 and 3, which is about 2.57, and the obtained C_u value is 10.27, which is greater than 6, respectively.

3.2.2 Sample Soils for Liquid Limit and Plastic Limit Test

The soil is jarred in a specific way, and the water content transforms from a plastic to a liquid form known as the Liquid Limit (L.L.). The water concentration at the transformation of plastic into a state is recognized as the Plastic Limit (P.L.). A grooving tool is utilized for spreading a soil sample portion in the L.L. machine's brass cup and dividing it for measuring the L.L. The L.L. is calculated after 25 drops, the moisture content after 1/2 inch, and the groove is closed. After 25 blows, the L.L. is shaped by a standard tool into a soil sample acquired in a standard manner, the standard cup closes for 10 mm. The cohesive soil converts the liquid to a plastic state by restricting moisture content.

Table 4 Liquid limit values for soil samples

Can No.	Empty wt. of Can	No. of Blows	Wt. of Can + Soil, (gm.)	Wt. of Can + Dry Soil, (gm.)	Water content (%)
C4	12.25	10	39.28	33.94	24.6
K3	24.82	36	53.36	48.56	20.27
C37	25.85	18	55.01	49.7	22.26
C30	22.18	26	46.67	42.4	21.11

Table 4 describes the liquid limit values for soil samples, it portrays the C4, K3, C37, and C30. It also shows the empty weight of the can, the number of blows, the weight of the can and soil, the weight of the can and dry soil, and the water content. The water content values for C4 are 24.6%, for K3 is 20.27%, for C37, the water content is 22.26%, and for C30 water content is 21.11%.

The plasticity limit is defined as the ratio of the moisture weight of the water and the dry weight of the soil. The formula for the plasticity limit is depicted as follows.

$$Plasticity\ Limit\ (Wp) = \frac{Weight\ of\ Water}{Weight\ of\ Dry\ Soil} \times 100\% \quad (4)$$

Where the weight of water is 1.36 gm, dry soil weight is 9.37 gm; therefore, water content is$\left(\frac{1.36}{9.37}\right) \times 100\% = 14.51\%$. Plastic limit $\left(W_p\right) = \frac{(14.51+14.59)}{2} = 14.55\%$ for an average of both values.

Weight of moisture recorded the weights for wet and dry of numerical difference. The dry weight of the sample is utilized for dividing and multiplying by 100% moisture to measure the "weight of moisture." Then the liquid limit (W.L.) is calculated at 25 blows using the moisture content, and the associated number of blows for the two liquid limits is determined. Divide the sample's moisture content by one of the denominators. It also shows the empty weight of the can, the number of blows, the weight of the can and soil, the weight of the can and dry soil, and the water content. The water content values for C4 are 24.6%, for K3 is 20.27%, for C37, the water content is 22.26%, and for C30 water content is 21.11%. Then the average value of the liquid limit is 21%.

A numerical variance between its Liquid and Plastic Limits is defined as the soil's Plasticity Index (P.I.), which is expressed as follows.

$$P.I = W_L - W_p \quad (5)$$

Table 5 Plastic limit values for soil samples

Can No.	Empty wt. of Can, (gm.)	Wt. of Can + Soil (gm.)	Weight of Can + Dry Soil (gm.)	Water content (w) %
41	22.07	32.8	31.44	14.51
47	15.6	23.14	22.18	14.59

Table 5 illustrates the plastic limit of soil samples which depicts can.no 41 and 47. The weight of water is 1.36 gm, and dry soil weight is 9.37 gm, therefore, water content is $(1.36/9.37) \times 100\% = 14.51\%$. Plastic limit $\left(W_p\right) = (14.51 + 14.59)/2 = 14.55\%$ for an average of both values. Based on the Indian Standard Soil Classification's plasticity chart.

$$P.I = 21\% - 14.55\% = 6.45\% \quad (6)$$

3.2.3 Permeability Test for Soil Samples

A variety of methods, including constant and falling head laboratory experiments on reconstituted or intact specimens were utilized for

determining soil permeability, it is also represented as hydraulic conductivity. Alternatively, in-situ borehole permeability testing and field pumping tests can be utilized to regulate permeability in the field.

Falling Head Laboratory Test: A prominent laboratory test for fine-grained soils with low and moderate permeability is the falling head permeability test (F.H.P.T.), such as clays and silts. To an undisturbed sample, this testing scheme can be applied. To changes in porosity, the test is not sensitive, and a high dispersion is occurring in this test. For each sort of test, determine a minimum number of repetitions. Permeability testing like pumping and borehole in the field; empirical connections between grain size distribution; oedometer test evaluation; and laboratory of permeability experiments on soil specimens are the four most common methods for calculating the permeability coefficient (hydraulic conductivity).

This classification of the Soil sample is denoted as "SM-SC." Classification of Soils like Silt, Clay, and Sand is S.M. The diameter of the Permeameter D is 7.20 mm. Diameter of Burette d is 1.10 mm. Area of a cross-section of Burette $= 0.950\ mm^2$. The area of the cross-section of the permeameter is $= 40.723\ mm^2$. The height of the fall H is 10 cm, Length of the sample L is 15 cm. Simultaneously, $h_0 = 76.5\ cm$ and $h_1 = 66.5\ cm$.

The permeability test results for the falling head represented the elapsed time that varies between 146.65 sec to 152.12 sec for the falling head as 10 cm. Based on the test findings depicted in the following equation, the permeability of soil samples is calculated:

$$K_{sat} = 3.27 \times 10^{-4}\ cm/sec \qquad (7)$$

The combination of Cylinder weight and Dry Soil sample is 1543 gm. Here, the weight of the Cylinder is 621.5 gm. It depicts the weight of the mixture in the Cylinder as 921.5 gm. The Volume of the Cylindrical Mould is 610.8 cc. The dry unit weight is $\gamma_{dry} = \frac{921.5}{610.8} gm/cc = 1.51$gm/cc $= 14.8$ KN/m^3. After completing the experiment of the permeability test, the weight of the Cylinder and saturated soil is calculated as 5256 gm. The observed weight of the Cylinder is 4166 gm, following that the weight of the saturated soil is $(5256 - 4166)gm = 1090\ gm$. Further, the saturated unit weight is of about $\gamma_{sat} = 1090/610.8\ gm/cc = 17.5\ KN/m^3$.In addition, the cohesion C value was 0.4 KPa, the internal friction angle ϕ is 25.45°, Young's modulus of Elasticity E is 5110 KPa, and the Poisson's ratio ϑ is 0.25, which is portrayed in table 2.

3.2.4 Direct Shear Test on Soil Sample

The soil materials' shear strength is assessed by the DST to construct a stress-strain curve for each test specimen, various normal stresses are usually three test specimens from the same sample were subjected. By reversing the lateral force later shearing the soil specimen, residual shear strength is assessed by some direct shear machines. Allow the water pressure for pores during soil DST to disperse through porous stones. The soil layer's weakest plane may not be represented by the failure plane due to the limited height of samples and the direct shear specimen's narrow shear plane. For trimming samples of thin-walled tube samplers that haven't been disturbed (Shelby tubes), the standard size of a shear box diameter of 2.5 in 63.5mm is portrayed in figure 11. When the shear specimen is installed in the shear box, while lateral or normal loading, filter paper inserts in porous stones are put on both the upper and lower surfaces to allow the water pressure for pore dissipation.

After inserting the shear box into the shear device, a little normal load is applied for seating. Apply the primary normal load, either progressively or in one step, after the components are properly aligned, and drench the sample in water. To determine consolidation, deformation is recorded consistently, and the load increments are applied at intervals of up to 24 hours. During horizontal loading, the shear rate is illustrated by the time and deformation data collected during this phase. A slow shear rate is required for prior failure to dissipate any substantial pore pressures. The normal stress is also connected to the errors between the test and corrected shear stress levels, according to the study of silty clay direct shear test findings.

For sample test 1, Normal Stress $\sigma = 0.5\ kg/cm^2$, Strain Rate = 0.25 mm/min. The failure shear load is 0.093 KN, the dimension of the shear box is $6cm \times 6cm$, and the corrected area of the Shear box at the failure area is about $6 \times (6 - 0.660)cm^2$. Therefore, the area corrected is $32.04cm^2$ and the failure shear stress is about $\tau_f = 93/(9.81 \times 32.04)Kg/cm^2 = 0.29588\ Kg/cm^2$.

Table 6 Plot of normal stress vs. shear stress

Shear Stress (τ), K.N./m^2	Normal Stress (σ), K.N./m^2
51.993	98.10
42.97	78.48
29.03	49.05

Table 6 shows the readings of shear stress and normal stress. The normal stress is 98.10 KN/m^2, 78.48 KN/m^2, and 49.05 KN/m^{2,} and the S.S. are 51.993 KN/m^2, 42.97 KN/m^2, and 29.03 KN/m^{2,} respectively. The parameters of shear strength are $\phi = 25.1°$ and $C = 7.5KN/m^2$. The normal stress and the strain rate for sample test 2 is 78.48 KN/m^2 and $0.25mm/min$; due to this, the shear load and shear stress (S.S.) failure is 0.133 kN and 42.97 kN/m^2. Due to the soil sample test 3, the normal stress and the strain rate are 98.1 kN/m^2 and $0.25mm/min$, then the failure shear load and failure shear stress are 0.160 kN and 51.993 kN/m^3.

Through more precise effective stress and shear strength estimations, pore pressure data can be used to reduce the uncertainty in slope stability. By improving the estimated pore pressure field, the updated hydraulic conductivity field changes the effective stress field. The strength parameters can also be updated utilizing the cross-correlation between the hydraulic conductivity and strength parameters. It should be noted that the increase in the mean F.O.S. is due to the specific distribution of pore pressures within the foundation layer and the resulting changes in shear strength; for a different spatial distribution of pore pressure, the mean F.O.S. could be reduced using updated pore pressure simulations.

The hydraulic head is determined as $h = z + \rho/\gamma_w$, in which z is the elevation, ρ is the pore pressure and γ_w is the unit weight of water, and k_x, k_y are the hydraulic conductivity in the x and y directions, respectively.

Table 7 Experimental deformation of slope at different effective angles

Effective Slope	Maximum Deformation (mm)
2:1	12.5
1.5:1	17.7
1.25:1	33.8

Table 7 demonstrates the maximum deformation at the different effective slopes of 2:1, 1.5:1, and 1.25:1. When the embankment slope is 2:1, the maximum deformation is 12.5 mm, when the embankment slope is 1.5:1, the maximum deformation is 17.7 mm, and the embankment slope is 1.25:1, then the maximum deformation is 33.8 mm. The formula for deformation is expressed as $x = F(X)$.

3.2.5 Numerical Modeling Using Geo-Studio 2021 Software

Geo-studio software is generally used for Slope analysis, Seepage analysis, and deformation analysis. It is based on the finite element method of analysis by utilizing this, the F.S. of slope can be determined at a different effective angle. By using SIGMA/W 2021 maximum deformation of the slope can be calculated, and after that, this can be compared with the experimental results. The F.S. of slope can be deliberate using SLOPE/W 2021. Here initially, seepage

analysis has been done by using SEEP/W 2021, and after that, it is utilized as a parent analysis in SLOPE/W and SIGMA/W for calculating the deformation vector, deformation mesh, and factor of safety.

Table 8 Factors of Safety at Different Embankment Slopes

Embankment slope	The factor of Safety (FoS)
2.25:1	1.349
2:1	0.973
1.5:1	0.826
1.25:1	0.686

Table 8 represents the F.S at different embankment slopes like 2.25:1, 2:1, 1.5:1, and 1.25:1. During an embankment slope is 2.25:1, then the F.S is 1.349 when the slope is 2:1, and the F.S is 0.973. The F.S. is 0.826 when the slope is 1.5:1, and the F.S. is 0.686 when the embankment slope is 1.25:1, respectively. After doing numerical modelling of a slope by using SLOPE/W 2021, the F.S. is derived. The equation for the factor of safety is given in the following equation (8),

$$Factor\ of\ Safety = \frac{Ultimate\ Load\ (Strength)}{Allowable\ Load\ (Stress)} \quad (8)$$

The allowable stress is always less than the ultimate failure stress, which is expressed from the above equation. Hence, the factor of safety is always greater than one, and the factor of safety at different effective angles is given below:

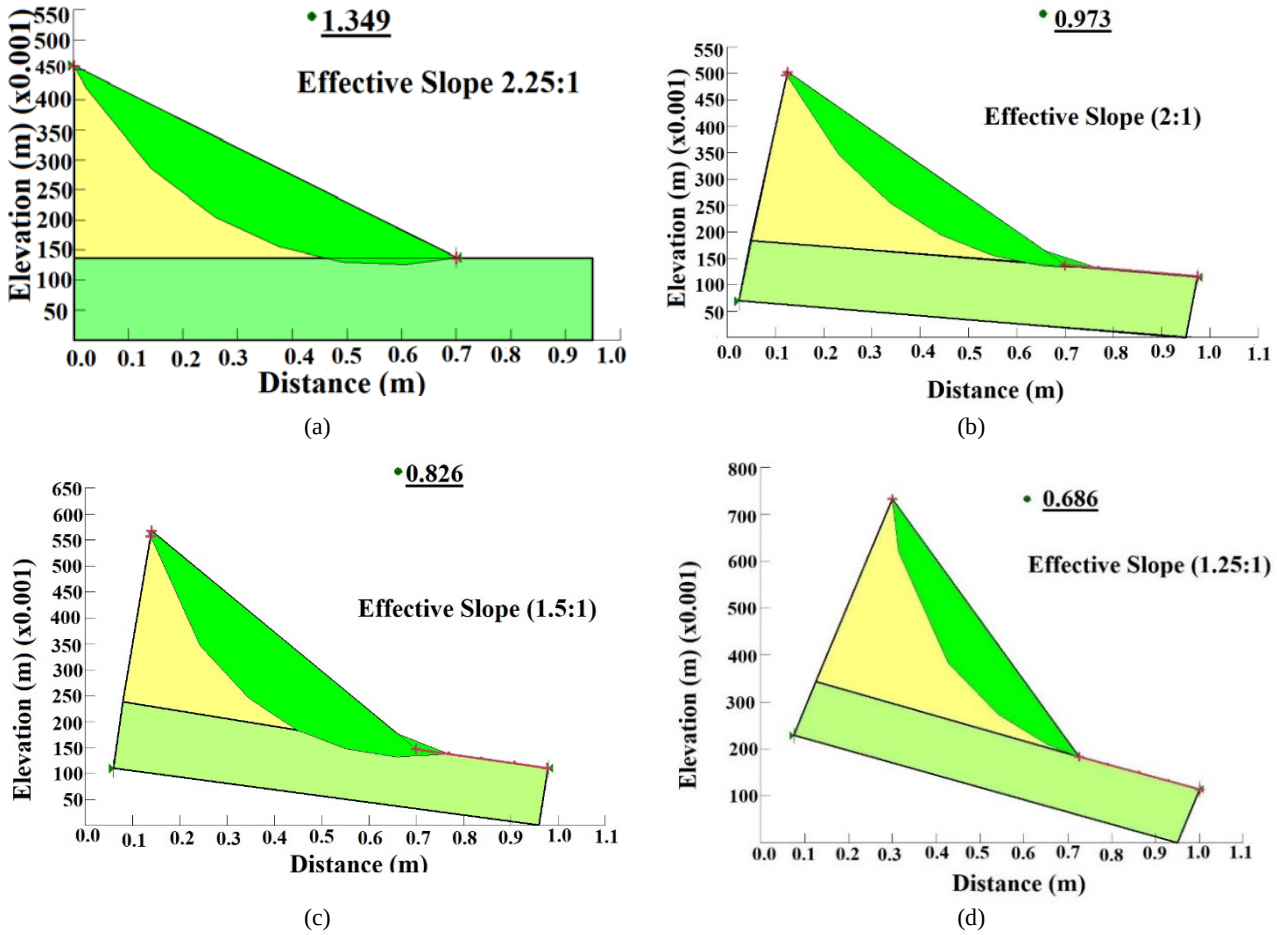

Figure 7 Factor of safety of slope at a different effective angle

Figure 7 depicts the factor of safety at a different effective angle. After doing numerical modelling of a slope by using SLOPE/W 2012, the factor of safety at a different effective angle is shown in figure 14. a) F.S of original slope (2.25:1) b) F.S at the effective slope (2:1) c) F.S at effective slope (1.5:1) d) F.S at the effective slope (1.25:1).

Table 9 Factors of safety at different effective slopes

Effective Slope	Factor of Safety (FoS)
2.25:1	1.349
2:1	0.973
1.5:1	0.826
1.25:1	0.686

Table 9 reveals the factor of safety at different effective slopes, 2.25:1, 2:1, 1.5:1, and 1.25:1. The factor of safety determined for these slopes are 1.349, 0.973, 0.826, and 0.686, respectively.

3.2.6 Deformation Analysis by Using Geo-Studio SIGMA/W 2021

To perform deformation and stress analyses of earth structures, a finite element CAD software product like SIGMA/W was utilized. Due to this complete formulation, it may be used to examine both basic and complex situations. A deformation examination has been completed at the different effective slopes for mesh deformation and vectors. Maximum deformation is recorded, and its value is compared by experimental data.

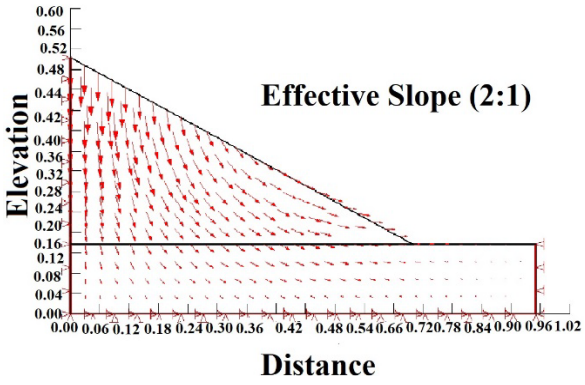

(a)

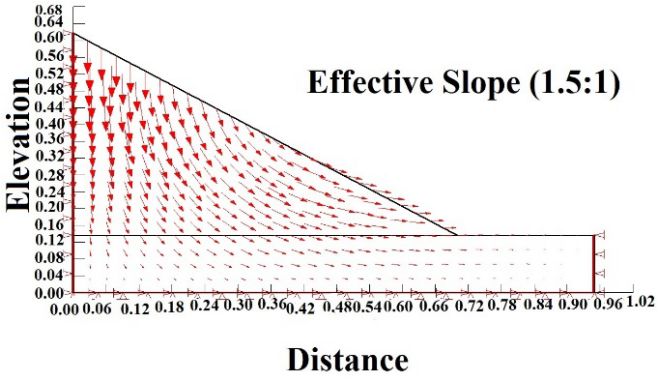

(b)

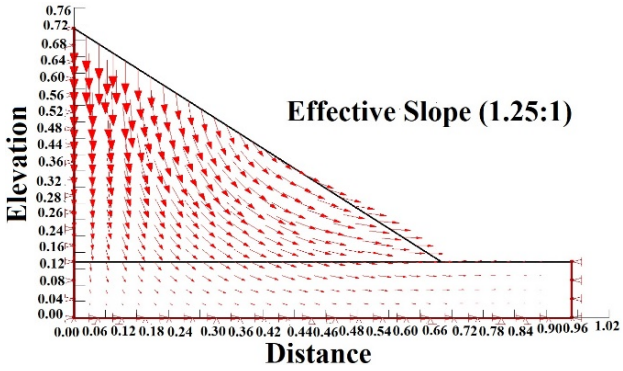

(c)

Figure 8 Vectors for different effective slopes

Figure 8 depicts the vector deformation model of effective slopes. (a) Vector deformation of effective slope (2:1) (b) Vector deformation of effective slope (1.5:1) (c) Vector deformation of effective slope (1.25:1).

Mesh Deformation for Different Effective Slopes

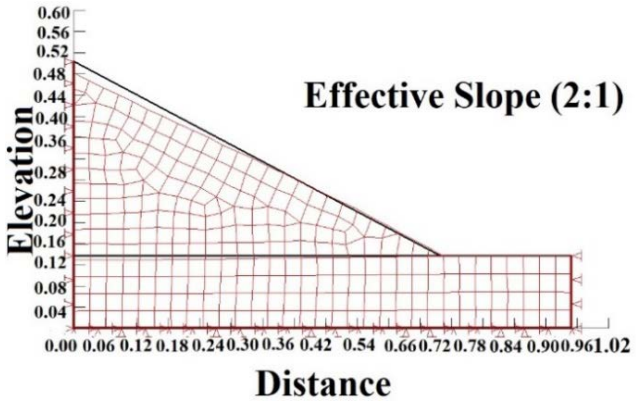

(a)

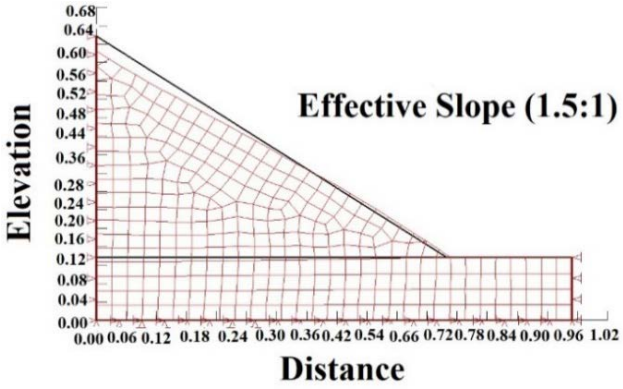

(b)

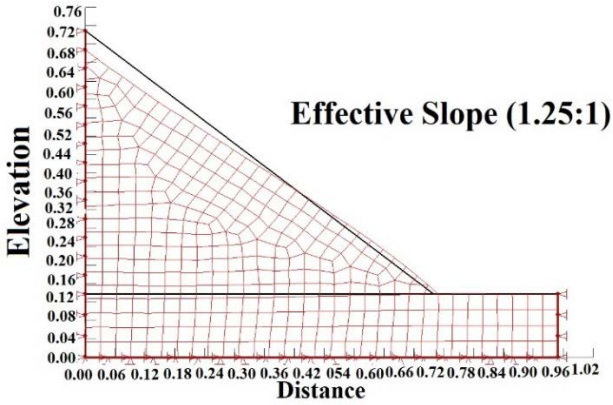

(c)

Figure 9 Mesh deformation of different embankment slopes

Figure 9 depicts the mesh deformation of different effective slopes. Figure 16 a) Mesh deformation of effective slope (2:1) b) Mesh deformation of effective slope (1.5:1) c) Mesh deformation of effective slope (1.25:1).

Table 10 Experimental and numerical deformation of slope

Effective Slope	Experimental Value (mm)	Numerical Value (mm)
2:1	12.5	11.2
1.5:1	17.7	15.9
1.25:1	33.8	25.7
Deformation of Slope at Field for $\lambda = 20$ (cm)		
2:1	16.6	22.4
1.5:1	29.4	31.8
1.25:1	59.6	51.4

Table 10 describes the experimental and numerical values for the deformation slope. The study took effective slopes of 2:1, 1:5:1, and 1:25:1, from which the experimental value is 12.5, 17.7, and 15.9; moreover, the numerical values are 11.2, 15.9, and 25.7 mm, respectively. Slope in the field of $\lambda = 20$, the experimental values are 16.6, 29.4, and 59.6 cm, and from the numerical simulation, the obtained values are 22.4, 31.8, and 51.4 cm, respectively. These obtained experimental and numerical values are slightly different for the slope deformation analysis.

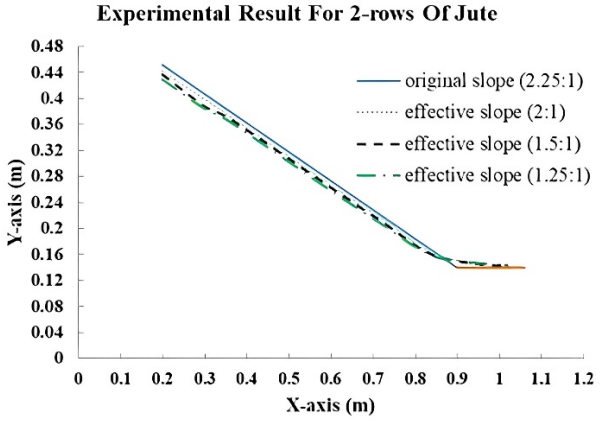

(a)

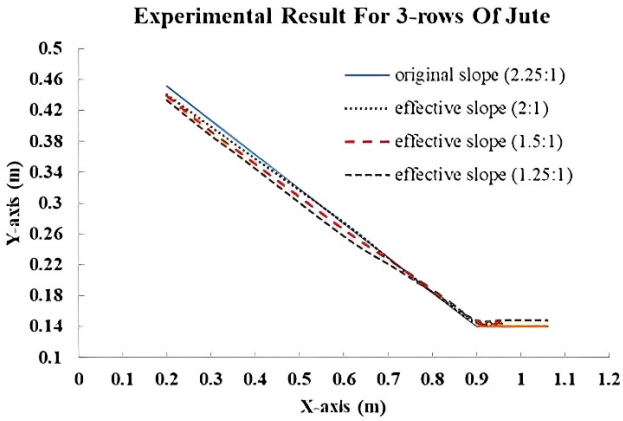

(b)

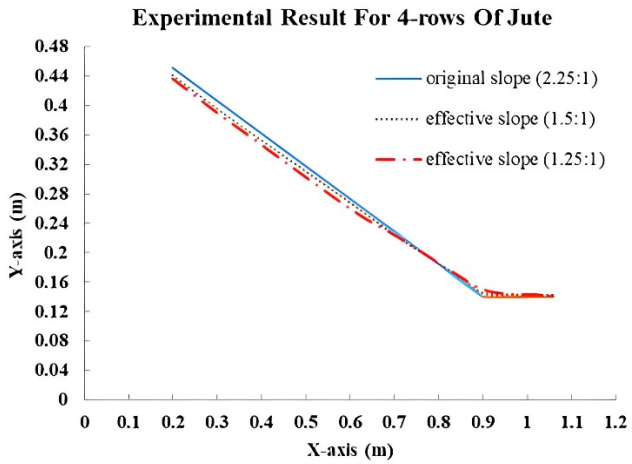

(c)

Figure 10 Experimental result for two, three, and four rows of jute

Figure 10 depicts the experimental results for two, three, and four rows of jute. Generally, the original slope is in the range of 0.14 to 0.451. For two rows of jute, the effective slope (2:1, 1.5:1, 1.25:1) experimental values from the original slope are in the range of 0.143 to 0.442. For three rows of jute fibre, the experimental values are in the range of 0.148 to 0441. Correspondingly, for five rows of jute fibre, the obtained values are in the range of 0.142 to 0.441, respectively.

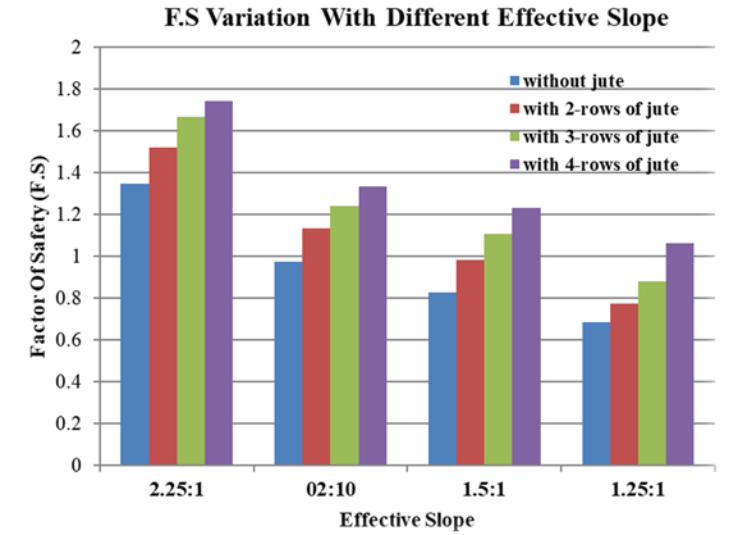

Figure 11 F.S for different embankment slopes

Figure 11 demonstrates the F.S. variation with the different embankment slopes. The figure depicts the effective slopes (2.25:1, 2:1, 1.5:1, and 1.25:1) factor of safety analysis for F.S. without jute, with two rows of jute, with three rows of jute, and with four rows of jute. Compared to the jute fibres, the F.S. without using jute fibres is very low than the two rows, three rows, and four rows jutes. The factor of safety produces a high value for the four rows jute. Thus, it depicts the factors using four rows of jute perform better than the other jute fibres or without using jute fibre, respectively.

Table 11 Mesh deformation values of experimental and numerical analysis using jute fiber

Effective Slope	Without Jute (mm)		With 2-Rows of Jute (mm)		With 3-Rows of Jute (mm)		With four rowsof Jute (mm)	
	Exp. value	Num. value	Exp. value	Num. value	Exp. value	Num. value	Exp. value	Num. value
2:1	12.5	9.8	10.6	7.6	8.5	5.6	4.4	2.3
1.5:1	17.7	14.6	16.6	13.7	13.4	7.8	9.6	4.6
1.25:1	33.8	25.8	29.2	22.4	24.8	14.6	18.5	11.8

Table 11 reveals the mesh deformation values for different effective slopes (2:1, 1.5:1, and 1.25:1) with the analysis of two rows, three rows, and four rows of jutes and without jute fibres. The experimentation and the numerical values are evaluated for these jute fibres with the embankment slope. It depicts that the mesh with fibres of jute is very low compared to those without jute, the analysts predict that the performance of using four rows. Jute is higher than the other fibres.

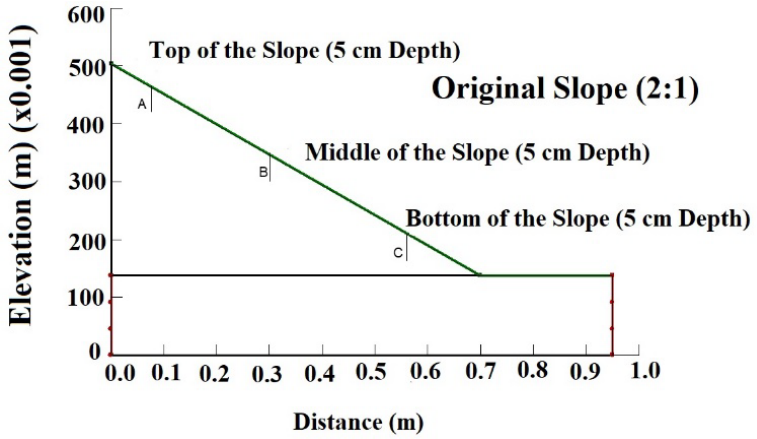

Figure 12 Matric suction graph

Figure 12 exhibits the matric suction graph for the original slope of 2:1. In this matric suction graph, the slope is divided into three types which include the top of the slope, the middle of the slope, and the bottom of the slope. The top of the slope is denoted as A, the middle of the slope is denoted as B, and the bottom of the slope is represented as C. In every layer of the slope, it takes 5 cm in depth, respectively.

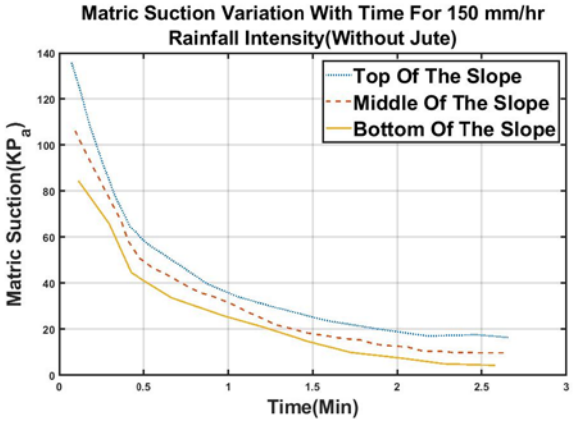

(a)

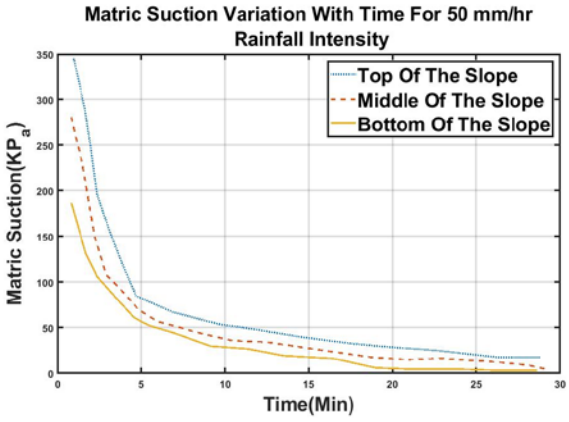

(b)

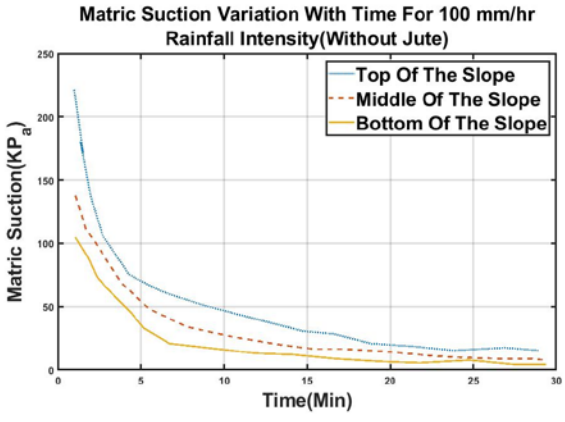

(c)

Figure 13 Matric suction variation with time

Figure 13 represents the variation of matric suction with time for the top, middle, and bottom of the slope. Figure 13 (a) portrays the matric suction variation with time for 50mm/hr rainfall intensity. The time suction for the top of the slope is 340 kPa, the middle of the slope was obtained as 280 kPa, and for the bottom of the slope, it was 191 kPa. Formerly the second figure (b) illustrates the matric suction variation with time for 100mm/hr rainfall intensity. Here, the slope values are 220 (top), 143 (middle), and 109 (bottom) kPa. After that, figure (c) depicts the matric suction variation with time for 150mm/hr rainfall intensity. From this figure, the slope values are obtained as 135 kPa for the top, 107 for the middle of the slope, and 80 for the bottom of the slope, respectively.

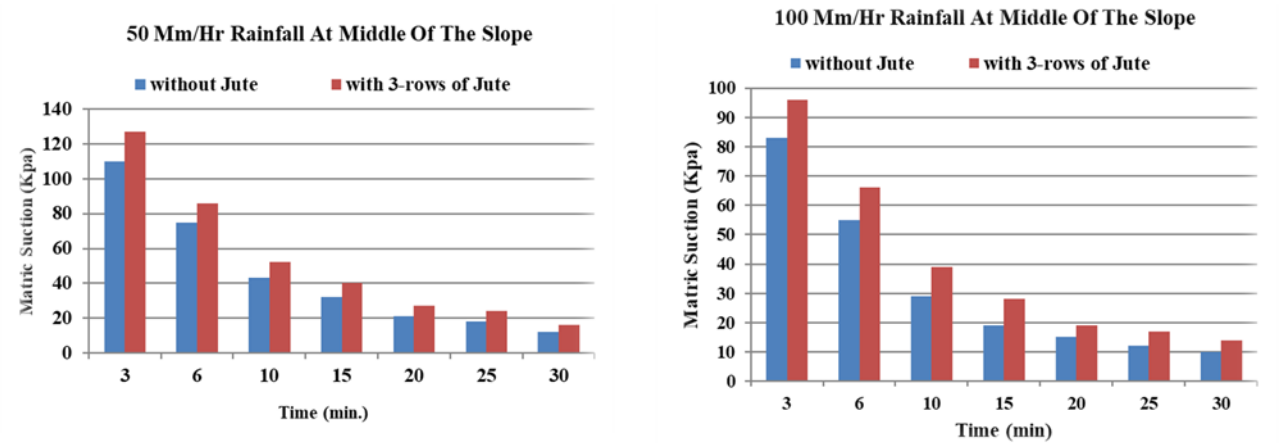

Figure 14 Matric suction comparison with and without Jute

Figure 14 depicts the matric suction comparison with and without jute at the middle of the slope. It predicts jute with row 3 performs better for the 50 and 100 mm/hr rainfall when compared to the without jute fibres. It is measured for the time of 3 to 30 minutes, and the matric suction value ranges from 0 to 130 KPa for the rainfall intensity of 50 mm/hr, and the matric suction value ranges from 0 to 100 KPa during the rainfall intensity of 100 mm/hr, respectively.

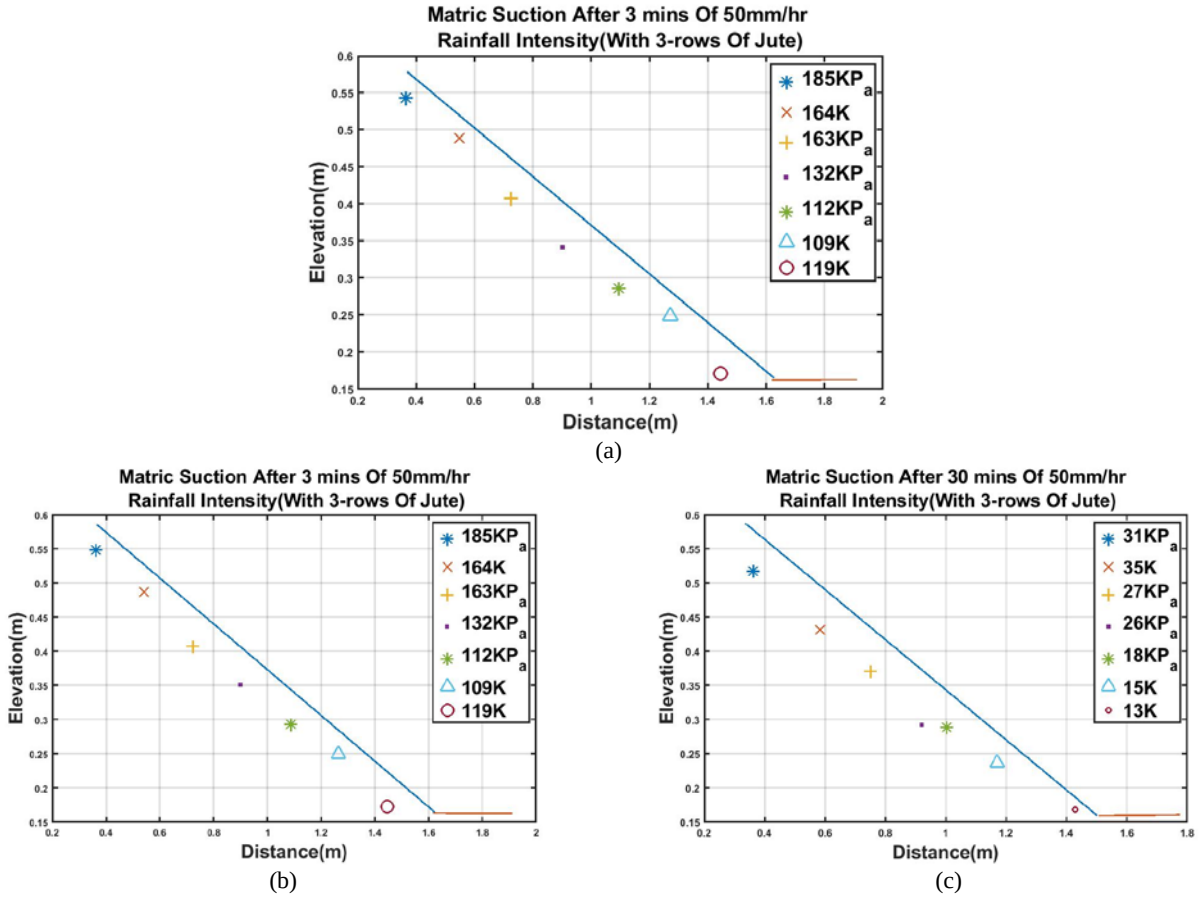

Figure 15 Matric suction with three rows of jute

Figure 15 demonstrates the matric suction variation values with three rows of jutes. The initial figure (a) shows the matric suction after 3 minutes of 50 mm/hr rainfall intensity with the three rows of jute. Then figure (b) reveals the matric suction after 10 minutes of 50 mm/hr rainfall intensity, and the final figure (c) depicts the matric suction after 30 minutes of rainfall intensity with the three rows of jute.

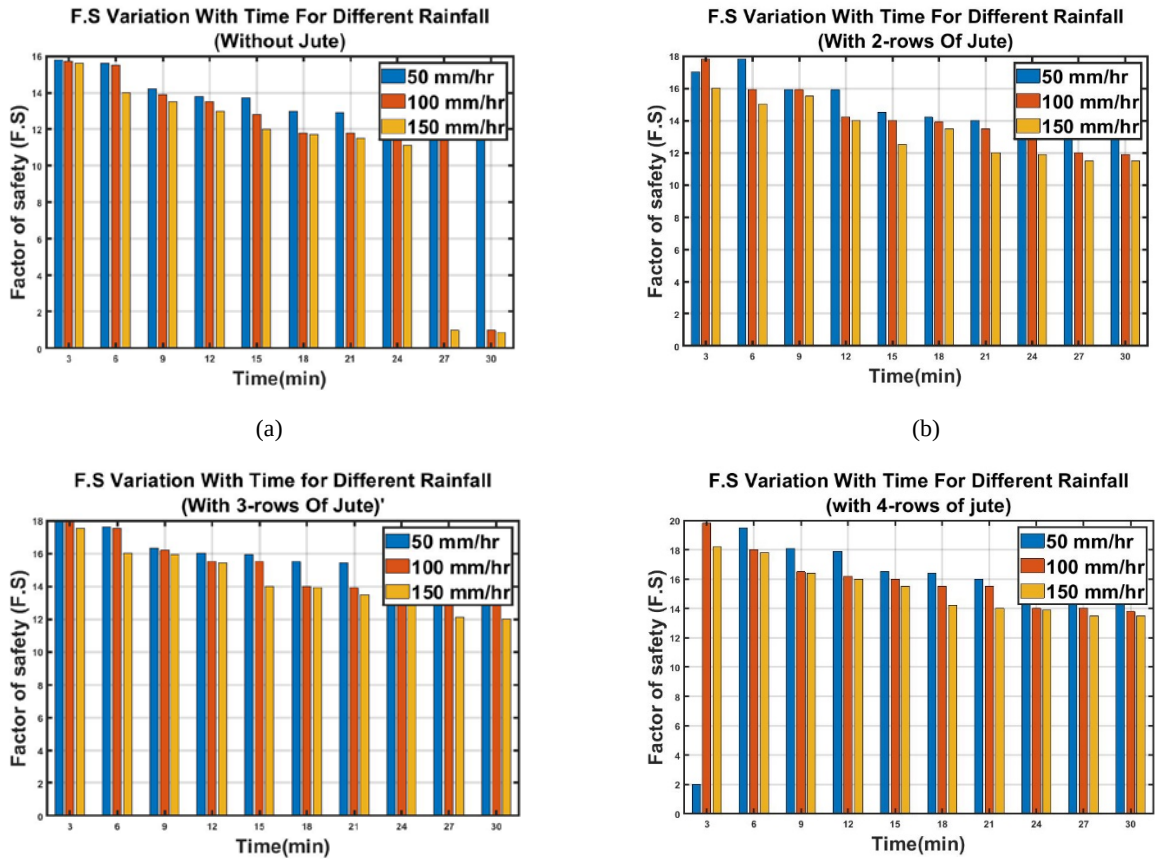

Figure 16 Factor of safety variation with and without jute

Figure 16 demonstrates the F.S. variation with two rows, three rows, and four rows jute and without jute. The F.S. variation for different rainfall intensity values is predicted for four types of jute fibre. Figure (a) shows the F.S. variation without using jute fibres in the embankment, and figure (b) reveals the F.S. variation with two rows of jute. Further, figure (c) illustrates the F.S. variation with three rows of jute, and figure (d) shows the F.S. variation with four rows of jute. Figure 34 clearly shows the factor of safety variation with time for different rainfall intensities, and it depicted that the performance of 4-row jute fibre is better than the other jute fibres and without using jute fibres.

4. CONCLUSIONS

Soil stabilization is very important for embankments, but the soils like clay and silt are weak soils for slope embankments. During rainfall, these soils produce cracks and slope failure because of this heavy rainfall. To overcome these problems, jute fibre is combined with the soil to improve soil stability. The experimental setup is constructed to test the slope stability of the soil samples. The rainfall intensity is used to assess the slope's stability, and several soil tests are carried out. Basic laboratory tests like sieve analysis, permeability test, direct shear test, liquid limit, and plasticity limit test were carried out to find the basic characteristics of soil samples collected from the site. During experimental and numerical analysis of slope stability, several cracks and deformations occurred in the tests. Due to this failure, the random inclusion of jute fibre effectiveness is assessed to strengthen the soil slope under heavy rainfall conditions. Here two rows, three rows, and four rows jute fibres are considered for the embankment slope for the analysis of the factor of safety and matric suction.

- According to the sieve analysis, the soil samples are well-graded and depict 27.17% of soil samples are silt and clay.
- These liquid limit and plasticity limit tests depicted that the liquid limit is 21%, the plasticity limit is 14.55%, and the plasticity index is 6.45%.
- Then the soil permeability test is performed with a dry unit weight is 14.8 kN/m^{3,} and a saturated unit weight is 17.5 kN/m^3.
- Due to the direct shear test for sample test 1, the normal stress is 0.5 Kg/cm^2, and the strain rate is 0.25 mm/min. Shear Load failure is predicted as 0.093 kN, and failure shear stress is 0.29588 Kg/cm^2. When the sample test 2, the normal stress is 78.48 kN/m^2, and the strain rate is 0.25 mm/min.
- Then the shear load and shear stress failure are 0.133 kN and 42.97 kN/m^2. While sample test 3, the normal stress and the strain rate are 98.1 kN/m^2 and 0.25 mm/min, and the sheer load and shear stress failure are 0.160 kN and 51.993 kN/m^2.
- Experimental results for slope deformation and factor of safety are determined, and the vector deformation and mesh deformation are expressed for the embankment slope of 2:1, 1.5:1, and 1.25:1. The deformation analysis is performed using Geo-studio SIGMA/W 2021 software.

- The real embankment dam was placed in a steady-state condition, and rainfall was applied to determine the impact of seepage and phreatic surface in the embankment dam.

Subsequently, the experimental results utilizing jute fibres for the factor of safety, mesh deformation, and matric suction is carried out in the test results. The comparison results have shown with the two rows, three rows, and four rows jute and without using jute fibre. The increase in soil strength characteristics suggests that fibres could be used in embankments for highway/road/dam projects. Numerical analyses were conducted to determine the feasibility of this application at the optimum fibre length that increased the embankment's F.O.S. As a result, when the slope is reinforced with fibres at the right proportion and length, the slope becomes more stable, and these four rows of jute fibre improves the embankment stability. In future, the study utilized different fibres to test the stability of the effective slope under rainfall and non-rainfall condition, respectively.

Data Availability Statement

No data, models, or code were generated or used during the study.

5. REFERENCES

Kassou, F., et al. (2020). "Slope Stability of Embankments on Soft Soil Improved with Vertical Drains." Civil Eng J. 6 (1), 164-173.

Farooq, Muhammad Umar, et al. (2020). "Evaluation of Stability and Erosion Characteristics of Soil Embankment Slope Reinforced with Different Natural Additives." *Iranian Journal of Science and Technology, Transactions of Civil Engineering*, 1-10.

Li, Lihua, et al. (2019). "Experimental Study of Embankments with Different Reinforcement Materials and Spacing Between Layers." *Geotextiles and Geomembranes*. 47(4): 477-482.

Kundu, Saroj, Subhra Sarkar, and Pritam Dhar. "Analysis of Slope Stability of Soil Using Fly-Ash & Lime."

Zhou, Haizuo, et al. (2019). "Performance of Embankments with Rigid Columns Embedded in an Inclined Underlying Stratum: Centrifuge and Numerical Modelling." *Acta Geotechnica*. 14(5): 1571-1584.

Abebe, Daniel Getachew (2020). "Determination of Effect of Moisture Content and Density on Shear Strength Parameters and Slope Stability of Highly Plastic Silt Embankment Soil (the Case of Wozeka-Gidole Road)."

Behnam Mehdipour, Behnam, et al. (2020). "An investigation into a Geocell-reinforced Slope in The Unsaturated Numerical Model." *Journal of Structural Engineering and Geo-Techniques.* 10(1): 1-14.

Wang, Yi-Xian, et al. (2017). "Laboratory Investigation on Strength Characteristics of Expansive Soil Treated with Jute Fibre Reinforcement." *International Journal of Geomechanics*, 17(11): 04017101.

Ramkrishnan, R., et al. (2018). "Soil Reinforcement and Slope Stabilization Using Natural Jute Fibres*." Civil Infrastructures Confronting Severe Weathers and Climate Changes Conference. Springer, Cham.*

Luo, Fangyue, Renlong Huang, and Ga Zhang (2020). "Centrifuge Modelling of the Geogrid-Reinforced Slope Subjected to Differential Settlement." *Acta Geotechnica*, 15(10): 3027-3040.

Kulhar, Kuldeep Singh, and M. Raisinghani (2017). "Shear Strength Performance of Sandy Soil Reinforced with Jute Fiber." *Journal of Basic and Applied Engineering Research, J.B.A.E.R.* 4(7): 624-629.

Dar, Naveed Anjum, and Gunjan Bhalla "Stabilization of Soil Using Jute Fiber and Stone Dust."

Sapkota, Anuja, et al. "Stabilization of Rainfall-Induced Slope Failure and Pavement Distresses Using Recycled Plastic Pins and Modified Moisture Barrier." *Geo-Congress 2019: Embankments, Dams, and Slopes*. Reston, VA: American Society of Civil Engineers, 2019.

Naidu, Shruti, et al. (2018). "Early Warning System for Shallow Landslides Using Rainfall Threshold and Slope Stability Analysis." Geoscience Frontiers, 9(6): 1871-1882.

Yang, Kuo-Hsin, et al. (2018). "Numerical Evaluation of Reinforced Slopes with Various Backfill-Reinforcement-Drainage Systems Subject to Rainfall Infiltration." *Computers and Geotechnics*, 96: 25-39.

Nguyen, T.S., Likitlersuang, S., Ohtsu, H. and Kitaoka, T. (2017). "Influence of the Spatial Variability of Shear Strength Parameters on Rainfall Induced Landslides: A Case Study of Sandstone Slope in Japan." *Arabian Journal of Geosciences*, 10(16), 369.

Nguyen, T.S., Likitlersuang, S. and Jotisankasa, A. (2019). "Influence of the Spatial Variability of the Root Cohesion on a Slope-Scale Stability Model: A Case Study of Residual Soil Slope in Thailand." *Bulletin of Engineering Geology and the Environment*, 78, 3337-3351.

Kumar, S. and Roy, L.B. (2022). "Rainfall Induced Geotextile Reinforced Model Slope Embankment Subjected to Surcharge Loading: A Review Study." *Archives of Computational Methods in Engineering*, 1-19.

Mamat, Rufaizal Che, et al. (2020). "Slope Stability Prediction of Road Embankment on Soft Ground Treated with Prefabricated Vertical Drains Using Artificial Neural Network." I.A.E.S. *International Journal of Artificial Intelligence*, 9(2): 236.

Li, Y.X., and X.L. Yang (2019). "Soil-slope Stability Considering Effect of Soil-Strength Nonlinearity." *International Journal of Geomechanics*, 19(3): 04018201.

Gong, Yafeng, et al. (2019). "Stability Analysis of Soil Embankment Slope Reinforced with Polypropylene Fibre Under Freeze-Thaw Cycles." *Advances in Materials Science and Engineering*, 2019.

Luo, Fangyue, et al. (2018). "Centrifuge Modelling of the Geotextile Reinforced Slope Subject to Drawdown." *Geotextiles and Geomembranes*, 46(1): 11-21.

Wang, Zhaoyu, et al. (2020). "Slope Failure of Biotreated Sand Embankments under Rainfall Conditions: *Experimental Investigation and Numerical Simulation." Bulletin of Engineering Geology and the Environment*, 79(9): 4683-4699.

Sharma, Yagya, D. G. M. Purohit, and Sunil Sharma (2017). "Improvement of Soil Properties by Using Jute Fibre as Soil Stabilizer." *American Journal of Engineering Research*, 6(10): 123-129.

Park, Jaesung, et al. (2019). "Slope Stability Evaluation of an Agricultural Embankment by Statistically Derived Rainfall Patterns." *Paddy and Water Environment*, 17(3): 303-313.

Adimilli, V. and Godavarthi, V.R.S.R. (2022). "Bamboo Geocell for Prevention of Heavy Rainfall-Induced Soil Slope Failure." *Arabian Journal of Geosciences*, 15(12): 1-10.

"Shear Strength and Mesoscopic Characteristics of Basalt Fiber–Reinforced Loess after Dry–Wet Cycles." *Journal of Materials in Civil Engineering*, 34(6): 04022083.

Zhang, W.G., Wu, J.H., Gu, X., Han, L., and Wang, L. (2022). "Probabilistic Stability Analysis of Embankment Slopes Considering the Spatial Variability of Soil Properties and Seismic Randomness." *Journal of Mountain Science*, 19(5): 1464-1474.

Jirawattanasomkul, T., Ueda, T., Likitlersuang, S., Zhang, D., Hanwiboonwat, N., Wuttiwannasak, N., and Horsangchai, K. (2019). "Effect of Natural Fibre Reinforced Polymers on Confined Compressive Strength of Concrete." *Construction and Building Materials*, 223, 156-164.

Jirawattanasomkul, T., Likitlersuang, S., Wuttiwannasak, N., Ueda, T., Zhang, D., and Voravutvityaruk, T. (2020). "Effects of Heat Treatment on Mechanical Properties of Jute Fiber–Reinforced Polymer Composites for Concrete Confinement." *Journal of Materials in Civil Engineering*, 32(12), 04020363.

Jirawattanasomkul, T., Likitlersuang, S., Wuttiwannasak, N., Ueda, T., Zhang, D., and Shono, M. (2020). "Structural Behaviour of Pre-Damaged Reinforced Concrete Beams Strengthened with Natural Fibre Reinforced Polymer Composites." *Composite Structures*, 244, 112309.

Jirawattanasomkul, T., Minakawa, H., Likitlersuang, S., Ueda, T., Dai, J.G., Wuttiwannasak, N., and Kongwang, N. (2021). "Use of Water Hyacinth Waste to Produce Fibre-Reinforced Polymer Composites for Concrete Confinement: Mechanical Performance and Environmental Assessment." *Journal of Cleaner Production*, 292, 126041.

Nguyen, T.S., Likitlersuang, S., and Jotisankasa, A. (2018). "Stability Analysis of Vegetated Residual Soil Slope in Thailand under Rainfall Conditions." *Environmental Geotechnics*, *7*(5), 338-349.

Komolvilas, V., Tanapalungkorn, W., Latcharote, P., and Likitlersuang, S. (2021). "Failure Analysis on a Heavy Rainfall-Induced Landslide in Huay Khab Mountain in Northern Thailand." *Journal of Mountain Science*, 18(10), 2580-2596.

Ongpaporn, P., Jotisankasa, A., and Likitlersuang, S. (2022). "Geotechnical Investigation and Stability Analysis of Bio-Engineered Slope at Surat Thani Province in Southern Thailand." *Bulletin of Engineering Geology and the Environment*, 81(3), 84.

Maryanto, E.T., Setyawan, A., Maria, T.S.B. and Astuti, W. (2023). "Analysis of the Performance of Natural Composite Materials Reinforced with Sago Sheath Fibers as an Alternative Material in Overcoming the Effect of Urban Heat Islands on Buildings." *Buildings*, 13(1), 18.

Kumar, S. and Roy, L.B. (2022). December. "A Case Study on Various Developments of Soil-Reinforced Embankment Slope Stability with Natural Fibre Additives." *In Proceedings of the Institution of Civil Engineers-Engineering Sustainability* (1-17). Thomas Telford Ltd.